Chapter 4 Growth and Characteristics of In isoelectronic doping GaN:Mg

The group III-nitride semiconductors have recently attracted much attention owing to varieties of applications in blue, green light-emitting diodes, violet laser diodes, as well as in semiconductor light bulbs [1-4]. Despite the number of advances being achieved, the realization of high conductivity p-type GaN material still remains a challenge, which hampers the rapid development of nitride-based laser diodes and bipolar devices [5]. For wide-bandgap material, due to the inherited deep acceptor energy level feature, a poor doping efficiency is usually a result in such types of semiconductor. However, the situation is even worse for GaN. This is because the Mg-doping itself can generate lots of native defects, causing severe self-compensation effects on degrading the film properties. To enhance the hole concentration, several methods have been employed to prepare the p-GaN, including modulation doping, codoping of p-type dopants, ion-implantation of high density of shallow Be acceptors, and performing the growth in a hydrogen-free ambient in addition to dehydrogenation process. The isoelectronic doping technique had been used in growing III-V or II-VI compound semiconductors to reduce background carrier concentrations, deep trap levels, and dislocation density [6-8]. A similar tendency was also observed in the optical properties by introducing the isoelectronic impurity into the films. Unfortunately, the as-grown GaN:Mg films are semi-insulating and not p-type conductive because of passivation of Mg-H complexes [9,10]. Even after thermal treatment, the hole density still decreases from Hall measurements for higher Mg

concentrations. Since the binding energy of Mg acceptor is as large as 250 meV, thus only a small fraction of Mg acceptors can be activated to donate holes at room temperature [11]. In this chapter, we present an alternative way to prepare p-type GaN, by using isoelectronic indium codoped with Mg during the deposition. Clear improvements are found in terms of surface morphology and electrical properties when the film is also doped with In atoms. We also studied photoluminescence (PL) of p-type GaN that was deposited by codoping isoelectronic In with Mg as a function of temperature. The measured temperature dependence of the slow PL intensity decay reveals which may be ascribed to an energy barrier to impede the carrier in the shallow Mg levels relaxed into the valence band. After In atoms were added into GaN:Mg, the energy barrier became higher than that of p-GaN, that is associated with the reduction of Mg-H complex or native defects.

4.1 Isoelectronic In doped GaM:Mg

In order to investigate the isoelectronic In-doping effects on p-GaN, two series of samples were prepared. One was a Mg-doped GaN films. The other was the Mg-In codoped GaN. These films were grown on a 2" c-plane (0001) sapphire substrates at 1110 ℃ using the low pressure metalorganic chemical vapor deposition (LP-MOCVD) method with a horizontal reactor. The samples were prepared by a nominal two-step growth method. A 300 Å low-temperature GaN nucleation layer was first deposited at 520 ℃, followed by a direct growth of ~ 2 μm thick GaN:Mg layer without the introduction of a buffer layer between them. The growth procedure was depicted in Fig 4.1. For sample preparation, electronic grade trimethylgallium

(TMGa), ammonia (NH_3), and bis-cyclopentadienylmagnesium (CP_2Mg) were used as the Ga, N, and Mg source precursors, respectively. When isoelectronic In doping was needed, trimethylindium (TMIn) diluted with hydrogen was used. Using the secondary ion mass spectrometry (SIMS) calibrated with a Mg ion-implanted standard, the Mg solid concentrations were determined to be about 3.9×10^{19} and 2.8×10^{19} cm^{-3} for p-GaN and In-doped p-GaN, respectively.

The first series samples were of Mg-doped GaN films grown with a Cp_2Mg flow rate varied from 100 to 495 sccm (0.118 μmol/min to 0.585 μmol/min). The other series were GaN:Mg films co-doped with isoelectronic In atoms prepared under essentially the same growth conditions, except for introducing a constant TMIn flow rate of 25.5 μmol/min (250 sccm) concurrently during the sample preparation. The corresponding growth conditions were illustrated in Table 4-1.

Table 4-1 The growth condition of GaN:Mg and In-doped GaN:Mg samples

Step	Temperature	Time/ Thickness	Flow Rate			
			TMGa (μmole/min)	NH_3 (SLM)	CP_2Mg (SCCM)	TMIn (μmole/min)
Thermal Cleaning	1120 ℃	10 min	—	—	—	—
LT-GaN nucleation layer	520 ℃	300 Å	39.2	4	—	—
Annealing	1120 ℃	3 min	—	2	—	—
GaN:Mg layer	1100 ℃	1 hr.	86.3	4	100 ~ 500	—
GaN:Mg+In layer						25.5

We note that there was a dramatic change in the film surface morphology, as revealed by the SEM micrographs in Fig. 4-2. For the Mg-doped GaN, many pockmarks, as expected, were spread all over the entire surface, stemming presumably

from the large differences of the atomic size between the Ga and Mg constants [12,13].

Although the size of the defects varied with the Mg source flow rate, the corresponding density remained rather high, lying in the range of 10^8-10^9 cm^{-2}. On the other hand, as TMIn was added, the size and density of the defects decreased notably for the 100 sccm Mg-flow-rate sample. More striking results were observed on the films grown with higher Mg flow rates. They possessed a virtually featureless surface structure when codoped with In atoms. Consequently, the corresponding root mean squared surface roughness value improved from the typical 12.2-26.6 Å for conventional p-GaN films down to a value of 4.2 Å, when the film was doped with In. The progress in surface smoothness for In-doped p-GaN can be attributable at least partially to the better surface migration capability of In, as compared to that of Ga, on the growing interface [14,15], and partially to the strain release of In doping in the Mg-doped GaN sample, because of the fact that the atom size of In > Ga and that of Mg < Ga, which not only caries the growth to be in a layer-by-layer manner, but also effectively suppresses the induced dislocations, defects and stacking faults that commonly occur in the p-type GaN epitaxial layer. In Figure 4-3, we show the In doping effects on the Hall properties of p-type GaN films thermally annealed at 750 ℃ for 30 min as a function of the Mg source flow rate. The results for nominal Mg-doped p-GaN films are also included in this figure for comparison. In accordance with other reports, some of the typical electrical characteristics are observed for Mg-doped GaN films. The associated hole concentration increased initially with the Mg source flow rate, and tended to drop subsequently with a further increase of the Mg supply. The optimum carrier concentration and resistivity are 4.2×10^{17} cm^{-3} and 2.1 Ω-cm, respectively. In regard to those In-Mg codoped p-GaN films, their Hall

properties basically showed a very similar tendency to that of shown by the Mg-doped films. Nevertheless, the entire film quality is improved. The resulting hole concentration reached ~ 9.0×10^{17} cm^{-3} while the resistivity is reduced to 1 Ω-cm, indicating the good quality of our Mg-In codoped GaN film. From the published literatures, we learn that there are a number of factors that affect the hole concentration in p-GaN, which include the solid Mg concentration, the degree of self compensation, the hydrogen passivation effect, and crystalline quality degradation. Among them, the solid Mg concentration is no doubt the most fundamental factor in determining the Hall properties of p-type GaN. It has been reported that the measured hole concentration in p-GaN tends to increase with the Mg concentration, up to the optimum doping level of $2\text{-}4 \times 10^{19}$ cm^{-3}, depending on schematic design the reactor and various growth parameters. Beyond this point the doping efficiency drops significantly, due to a rapid increase in its donor concentration, which gives significant compensation effects in the film. Actually, the compensation seems inevitable for p-type GaN film, because the Mg doping itself can unintentionally induce native donor defects, with shallow-types dominating in the lightly doped samples and deep-types in the heavily doped ones. For this reason, we carried out a second set of ion mass spectrometry (SIMS) measurements. The SIMS data in Fig. 4-4 reveal that the solid Mg concentration increased monotonically with the Mg flow rate for conventional GaN:Mg films; on the other hand, a saturation characteristic was observed in our In-doped samples. The increasing of the solid Mg concentration with the Mg flux, together with a decrease in the hole concentration in the Mg-doped samples, suggests that our p-GaN films grown by the conventional method are all overdoped. The corresponding critical solid Mg concentration is conceivably not greater than 3.7×10^{19} cm^{-3}. As for the In-doped samples, the low measured Mg saturation value indicates that the Mg solubility is being suppressed to a certain extent

by the addition of In atoms, which can be partly credited to the increased competition of Mg atoms with In atoms in occupying the Ga sublattices. Based on the above arguments, we can infer that the increased holes concentration in In-doped p-GaN is not a direct result of an increasing Mg concentration in a solid, since an adverse effect is observed in our In-doped films. It is certain that the mechanisms involved in p-GaN are rather complex in nature; we believe this is also true for the In-Mg co-doped GaN case. Definitely the study of isoelectric doping effects on p-GaN is still in its infant stage. Full comprehension is currently impossible and is beyond the scope of our discussion here, due to the limited information available from the aforementioned measurements. Nonetheless, the phenomena induced by In-doping in p-type GaN can be ascribed at least qualitatively to the following reasons： First, the In doping in such types of film keep the solid Mg concentration apart, slightly away from the overdoped situation. This keeps the film from generating a large density of Mg-related deep-donors, thus avoiding the occurrence of severe compensation effects, so that better Hall properties can be obtained. Second, it is generally believed that the higher the dislocation density, the less the resultant carrier density in the epitaxial film. It has been shown that adding In to conventional GaAs bulk crystals can greatly reduce the density of dislocations by pinning the dislocations at In atoms due to a larger radius of In than Ga [16]. This seemingly is also the case for p-GaN, as revealed by SEM micrographs (Fig. 4-2), where a much smoother surface morphology can be obtained when the film has In added. If the surface density has an certain proportionality with the dislocation density, and hence with its extended point defect concentration, we may reasonably anticipate that we can developed a lower compensation ratio in our In-doped p-GaN film. Another likely effect caused by the In doping in p-GaN is the reduction of the nitrogen vacancy density. For In-containing alloys, we have found in our study that, regardless of the growth of GaN, InGaN or Mg-doped GaN the

introduction here of In atoms during the epitaxy can always bring a sudden decrease in the Ga incorporation efficiency. This yield means a higher effective V/III ratio on the growing interface, which believably could help in reducing the formation of nitrogen vacancies in the solid. Although not all of these samples are suitable for deep-level transient spectroscopy measurement, we do find in undoped GaN film a notable decrease in the nitrogen vacancies [17]. We believe similar results can also occur in In-doped p-GaN film. Since the nitrogen vacancy functions as a shallow donor in GaN film and represents the major intrinsic compensation center for Mg doping in the 10^{18} to 10^{19} cm^{-3} range. The decrease of nitrogen concentration could indubitably enhance the hole concentration in the valence band. Finally, it is known that hydrogen plays a key role in the p-type doping of GaN. When hydrogen is present in the solid, it passivates substitutional Mg by forming Mg_{Ga}-N-H complex, resulting in a poor doping efficiency in as-grown GaN. Experimental data indicate that, under a similar solid Mg concentration, a p-GaN film with a lower hydrogen concentration usually could possess a higher carrier concentration. This is also observed in our In-doped GaN film. In Fig. 4.5, we show a typical impurity incorporation depth profile for both pure Mg-doped and In-Mg codoped GaN films. One can note that the Mg concentrations are about the same for both types of the samples, while the hydrogen concentration in the In-doped sample appears to be ~ 50% lower than that of Mg-doped film. Although thermal annealing in ambient nitrogen can remove hydrogen from the complex to some extent, complete dehydrogenation is difficult to accomplish for GaN, because of the thermal budget limitation. That is under thermal treatment a certain portion of the hydrogen ions remains in the solid where they will again form an Mg-H complex during the cooling to room temperature which degrades the properties of the film [18]. Thus, for p-type GaN growth, perhaps a better way to obtain a high hole concentration would be to grow a film with a lesser degree of

hydrogen passivation. The less the hydrogen content, the higher the concentration of Mg atoms that can actively provide free holes to the valence band, and the better the device performance that can be obtained. Additionally, probably due to the lesser degree of hydrogen passivation, we did find some interesting electrical behaviors in our In-doped p-GaN. As shown in Fig. 4.6, a nearly ohmic I-V characteristic is readily attained in our as-deposited In-doped p-GaN film, which has seldom been reported by the MOCVD nitride community. For comparison, the typical characteristics of high resistivity and rectifying carrier transport behavior are observed, as expected, for our as-deposited Mg-doped GaN films.

4.2 TMIn Flow Rate Effect

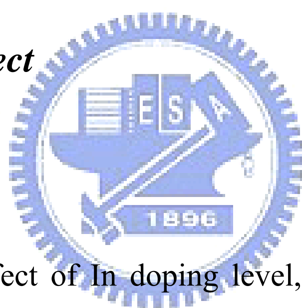

In order to study the effect of In doping level, another series of p-GaN films codoped with In doping levels were also prepared. As shown in Table 4-2.

Table 4-2 The growth condition of In-doped GaN:Mg samples with various TMIn flow rate

Step	Temperature	Time/ Thickness	Flow Rate			
			TMGa (μmole/min)	NH_3 (SLM)	CP_2Mg (μmole/min)	TMIn (SCCM)
Thermal Cleaning	1120 ℃	10 min	—	—	—	—
LT-GaN nucleation layer	520 ℃	300 Å	39.2	4	—	—
Annealing	1120 ℃	3 min	—	2	—	—
GaN:Mg+In layer	1120 ℃	1 hr.	86.3	4	0.296	0 ~ 400

The Raman spectra of both the p-GaN and In-doped p-GaN films were shown in Fig .4.7, the sapphire phonon modes at 415 and 748 cm^{-1} are clearly seen, which can be used as frequency marks. There are also distinct GaN E_2 and A_1(LO) modes at 567 and 734 cm^{-1}, respectively. If In atoms is alloyed with p-GaN films, one would expect to see the A_1(LO) mode broadening or merging with carrier induced plasmon [19]. But, we do not see such a behavior. The E_2 and A_1(LO) modes' position and width appear irrelevant to the amount of In atoms added to the In doped p-GaN films. These results imply that the In codoped samples are isoelectronic doping rather than alloying, because the maximum In atom incorporation into p-GaN film is less than 0.2 % (SIMS) in our samples. Note that, for the without In codoping Mg-doped samples, weak A_1(TO) and E_1(TO) features appear at 534 and 553 cm^{-1} on the low energy shoulder of the E_2 mode (567 cm^{-1}). In Fig. 4.7, the A_1(TO) and E_1(TO) features of the In codoping Mg-doped samples are much weaker than that of without In co-doping samples. It suggests that the selection rule from the (0001) surface is some what relaxed and the crystal orientation is not as good as the In doped films. As the TMIn flow rate increases, the sample looks more transparent and the elastic scattering from its surface is reduced significantly. At increasing the TMIn flow to 250 sccm, the A_1(TO) mode is no longer observable which indicates improved crystal orientation.

The result of PL spectra of GaN:Mg and In-doped GaN:Mg films obtained at room temperature are shown in Fig. 4.8. For the GaN:Mg sample, a broad band (blue emission) is observed at 430 nm (2.8 eV) which involves either shallow donor to Mg related deep levels or deep donor to common Mg acceptors [20]. In heavily Mg doped GaN, the broad band also indicates the likely overlapping of Mg-related deep trap centers and common Mg levels. As In atoms were added into GaN:Mg films, the PL

intensity of the band shoulder at 3.1 eV increased evidently then decreased. It had been reported that in lightly Mg-doped GaN, the band of 3.1 eV was attributed to a recombination between the electron in the conduction band and isolated Mg_{Ga} [21,22]. From the theoretical calculations [23,24], the only native defect with relevant concentration in p-GaN is nitrogen vacancy (V_N) and its concentration is nearly the same as the Mg concentration at commonly used MOCVD growth temperatures. The V_N and the Mg acceptor, which are oppositely charged, tend to form the Mg_{Ga}-V_N complex as the compensation centers [21]. For In-containing alloy, we have found in previous studies that regardless of the growth of GaN, InGaN or Mg-doped GaN, the introduction of In atoms during the epitaxy can always bring a sudden decrease in Ga incorporation efficiency [17,25,26]. This means that a higher effective V/III ratio is yielded on the growing interface, which believably helps reduce the formation of V_N in the solid [17,26,27].

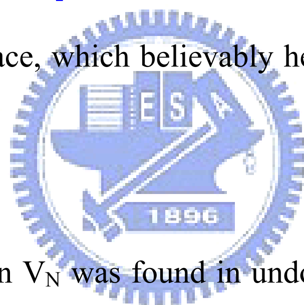

Since a notable decrease in V_N was found in undoped GaN film [17], we believe that similar results can also occur in In-doped p-GaN film leading to Mg_{Ga} concentration increase. This is why the 3.1 eV transition emerges and the 2.8 eV donor-acceptor pair transition weakens after doping In into GaN:Mg. As the TMIn flow rate increased to 400 sccm, the multiple interference effect of the PL spectra becomes less evident that may be due to non-flat surface. Apparently, the In incorporation of proper amount can reduce the self-compensation centers by native defects. The excess In atoms probably play the role of the luminescence killer. Since the surface migration rate of In is higher than that of Ga, In atoms may occupy Ga site and form the radiation killer [28]. The cause for such radiation quenching is still unknown and needs more studies. However, too much incorporation of In atoms indeed caused film deterioration, similar to that of In over-doped GaAs and GaP

[8,16,29].

Under continuous excitation ($>$680 W/cm^2), the PL intensity decays with rather long time constants. We show the typical PL intensity evolutions from 380 to 420 nm for p-GaN and In-doped p-GaN films were shown in Fig. 4.9. The luminescence intensity shows drastic changes below 420nm, which reflect different mechanisms for the 3.1 and 2.8 eV emissions. In the p-GaN, the photo-excited electrons will relax to the conduction band minimum or the shallow donor levels and then recombine with holes in both shallow Mg_{Ga} acceptor and deep Mg level. The fast recombination ($<$ 420 nm) is resulted from the photon excited carriers being captured by the impurity center with associated deep Mg levels. After In atoms were added into p-GaN, the intensity decay became rather slow for short wavelength ($<$ 420nm). Under continuous photon pumping, the electrons trapped in shallow Mg_{Ga} acceptors may rapidly relax or may be re-excited to the conduction band so that the recombination rate remains large. Thus the slow decay indicates that the transition probability increases between the conduction band (shallow donor) and the shallow Mg acceptors.

The long time decay behavior can be modeled by radiative transitions between two levels. For an approximate solution, we adopt the following equation of exponential form for the population number,

$$p(t) = p_0 e^{-t/\tau} \quad , \qquad (1)$$

where p_0 is the initial population number. τ is the decay time constant. Assuming that

the PL dynamic response is proportional to the population *p(t)*, then

$$I(t) = I_0 e^{-t/\tau} \quad , \qquad (2)$$

The fitted time constants from 380 to 420 nm for p-GaN and In doped p-GaN are shown in Fig. 4.10. For emission below 410 nm, the decay time constants of In-doped p-GaN was large than that of p-type GaN. Our results suggest that the In-doped p-GaN film has higher energy barrier than Mg-doped p-GaN to increase the decay time constant. In persistent photoconductivity (PPC) effect, there has been reported that H passivation may be responsible for the nonequilibrium process of the dark conductivity [30,31]. We believe that the higher energy barrier in In-doped p-GaN could be associated with the reduction of the impurity defects, such as isolated H atoms or Mg-H complexes. Our SIMS data also supported that H-concentrations are reduced effectively by doping In into p-GaN [32].

In addition to the potential barrier effect, the density of states of Mg_{Ga} increase was another reason for the long decay time below 410 nm. For Mg doped GaN, the defect complex like that V_N-Mg_{Ga} will form the self-compensation center as described before. When In atoms are added into the p-GaN films, the density of V_N in the solid will be reduced by the growing interface with higher effective V/III ratio that increases the Mg_{Ga} concentration. Then by photo pumping, the transition probability of carriers from the conduction band or shallow donor to shallow Mg_{Ga} acceptor levels would remain relatively steady and cause long decay time constants (τ).

The PL intensity evolution at 400 nm for In (250sccm) sample is shown in Fig.

4.11 as a function of temperature that reveals the energy barrier effect. For temperatures below 110 K, the PL intensity decays slowly. They are due to nearly constant occupied action number states in the Mg-related levels and the holes are sufficient for recombination. Because the thermal energy is too low to overcome the energy barrier of the shallow Mg acceptor states. The fast decay time for temperatures higher than 110 K is because the thermal energy allows the holes in the shallow Mg acceptor to be excited to the valence band. At the low temperature, the population number is nearly constant and the carriers are sufficient to increase the transition probability. At the high temperature, the population number and recombined carriers would decrease due to thermal excitation. On another words, the probability of available holes for radiative recombination is reduced at higher temperatures. On the other hand, the probability of available holes for radiative recombination is reduced at higher temperatures. An Arrhenuis plot of the inverse decay time constant vs. inverse temperature is shown in the inset of Fig. 4.11 that can be described by [33,34],

$$\frac{1}{\tau} \propto \exp\left(-E_b/kT\right) \tag{3}$$

where E_b is the barrier energy for holes of Mg-related levels being ionized into the valence band. The barrier energies of 69±8, 90±5, 103±7, 88±5 meV are obtained for p-GaN and In-doped p-GaN, respectively. Indeed, an optimal In-doping induces the highest barrier energy and thus the longest decay time.

References

1. S. Strite and H. Morkoc, *J. Vac. Sci. Technol. B* **10**, 1237 (1992).
2. S. Nakamura, M. Senoh, S. Nagahama, N. Iwasa, and S. Nagahama, *Jan. J. Appl. Phys.*, Part 2, **34**, L797 (1995).
3. M. Harada, Nikkei, *Electronics Asia, NEW/Focus*, December, 30 (1997).
4. S. Nakamura, M. Senoh, S. I. Nagahama, N. Iwasa, T. Yamada, T. Matsushita, Y. Sugimoto and H. Kiyoku, *Appl. Phys. Lett.* **70**, 866 (1997).
5. H. Amano, M. Kito, K. Hiramatsu, and I. Akasaki, *Jpn. J. Appl. Phys.* **28**, L2112 (1989).
6. D. G. Thomas, J. J. Hopfield and C. J. Frosch, *Phys. Rev. Lett*. **15,** 857 (1965).
7. K. Akimoto, H. Okuyama, M. Ikeda and Y. Mori, *Appl. Phys. Lett.* **60,** 91 (1992).
8. W. Walukiewicz, *Appl. Phys. Lett*. **54,** 2009 (1989).
9. S. Nakamura, N. Iwasa, M. Senoh, and T. Mukai, *Jpn. J. Appl. Phys*. **31,** 1258 (1992).
10. W. Gotz, N. M. Johnson, J. Walker, D. P. Bour, H. Amano, and I. Akasaki, *Appl. Phys. Lett*. **67,** 2666 (1995).
11. S. Fischer, C. Wetzel, E. E. Haller, and B. K. Meyer, *Appl. Phys. Lett*. **67,** 1298 (1995).
12. Yaso Ohba, Ako Hatano, *Jap. J. Appl. Phys*. **33**, L1367 (1994).
13. W. Götz, N. M. Johnson, J. Walker, D. P. Bour, and R. A. Street, *Appl. Phys. Lett.* **68**, 667 (1996).
14. C. K. Shu, J. Ou, H. C. Lin, W.K. Chen, and M. C. Lee, *Appl. Phys. Lett*. **73,** 641 (1998).
15. H. Beneking, P. Narozny, and N. Emeis, *Appl. Phys. Lett*. **47**, 828 (1985).
16. P. K. Bhattacharya, S. Dhar, P. Berger, and F.-Y. Juang, *Appl. Phys. Lett*. **49**,

470 (1986).

17. H. M. Chung, W. C. Chuang, Y. C. Pan, C. C. Tsai, M. C. Lee, W. H. Chen, and W. K. Chen, *Appl. Phys. Lett*. **76,** 897 (2000).

18. J. A. van Vechten *et al*., *Jan. J. Appl. Phys*. **31**, 3662 (1992).

19. Kosawa, T. Kachi, H. Kano, Y. Taga and M. Hashimoto, *J. Appl. Phys*. 75, 1098 (1994)

20. J. M. Myoung, K. H. Shim, C. Kim, O. Gluschenkov, K. Kim, S. Kim, D. A. Tumbull and S. G. Bishop, *Appl. Phys. Lett*. **69,** 2722 (1996).

21. U. Kaufmann, M. Kunzer, M. Maier, H. Obloh, A. Ramakrishnan, B. Santic, and P. Schlotter, *Appl. Phys. Lett*. **72,** 1326 (1998).

22. J. K. Sheu, Y. K. Su, G. C. Chi, B. J. Pong, C. Y. Chen, C. N. Huang, and W. C. Chen, *J. Appl. Phys*. **84,** 4590 (1998).

23. J. Neugebauer and C. G. Van de Walle, *Phys. Rev. B* **50,** 8067 (1994).

24. J. Neugebauer and C. G. Van de Walle, *Appl. Phys. Lett*. **68,** 1829 (1996).

25. J. Ou, W. K. Chen, H. C. Lin, Y. C. Pan, and M. C. Lee, *Jpn. J. Appl. Phys*. **37,** L633 (1998).

26. C. K. Shu, J. Ou, H. C. Lin, W.K. Chen, and M. C. Lee, *Appl. Phys. Lett*. **73,** 641 (1998).

27. H. Y. Huang, C. K. Shu, W. C. Lin, C. H. Chuang, M. C. Lee, and W. K. Chen, *Appl. Phys. Lett*. **76** (2000) 3224.

28. H. Beneking, P. Narozny and N. Emeis, *Appl. Phys. Lett*. **47** (1985) 828.

29. M. K. Lee, T. H. Chiu, A. Dayem, and E. Agyekum, *Appl. Phys. Lett*. **53,** 2653 (1988).

30. C. Johnson, J. Y. Lin, H. X. Jiang, M. Asif Khan, and C. J. Sun, *Appl. Phys. Lett*. **68,** 1808 (1996).

31. J. Z. Li, J. Y. Lin, H. X. Jiang, A. Salvador, A. Botchkarev, and H. Morkoc,

Appl. Phys. Lett. **69,** 1474 (1996).

32. F. C. Chang, K. C. Shen, H. M. Chung, M. C. Lee, W. H. Chen and W. K. Chen, *Chin. Jour. Phys*. **40**, 637 (2002).
33. A. Dissanayake, am. Aelahi, H. X. Jiang, and J. Y. Lin, *Phy. Rev. B* **45,** 13996 (1992).
34. J. Y. Lin, A. Dissanayake, G. Brown, and H. X. Jiang, *Phy. Rev. B* **42,** 5855 (1990).

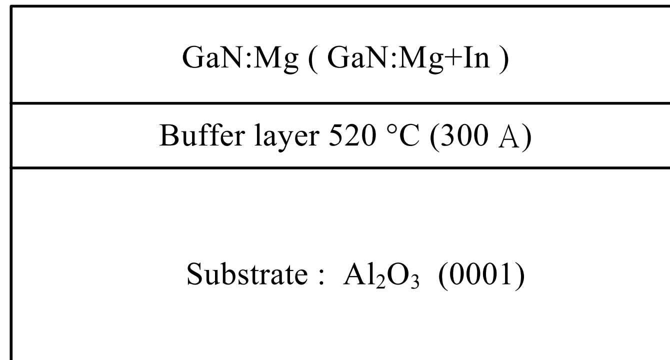

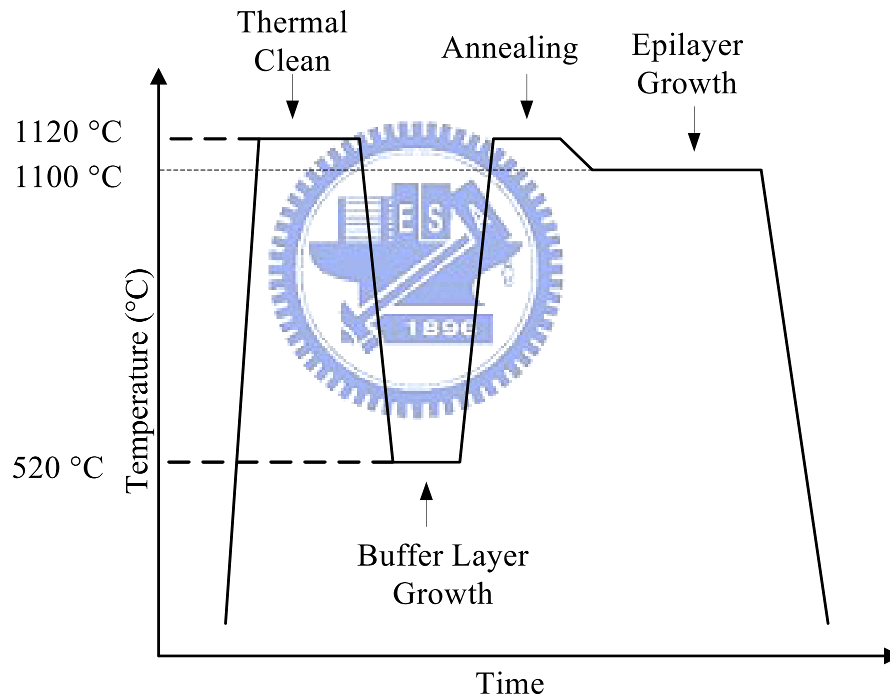

Fig 4.1 The schematic diagrams of GaN:Mg(+In) structure and the corresponding growth procedure.

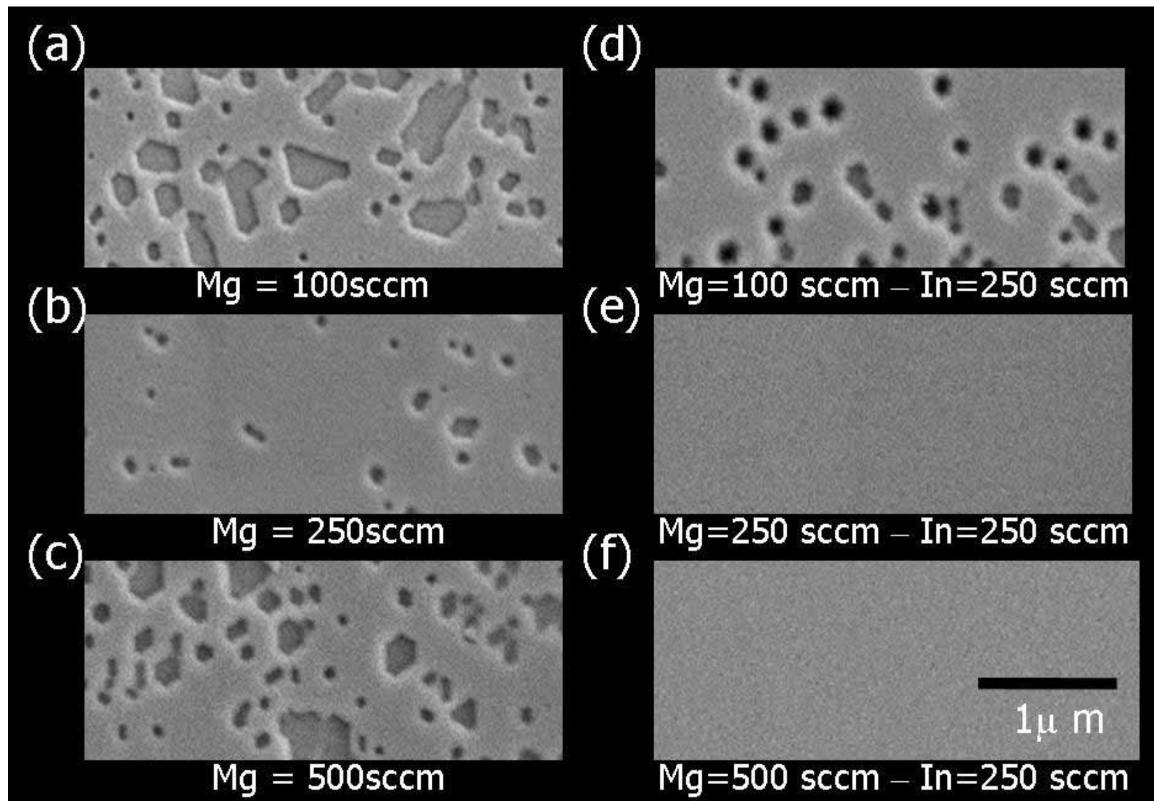

Fig. 4.2. SEM micrographs of (a) ~ (c) for GaN:Mg films grown with various Cp_2Mg flow rates from 100 to 495 sccm, and (d) ~ (f) for GaN:Mg films co-doped with In atoms.

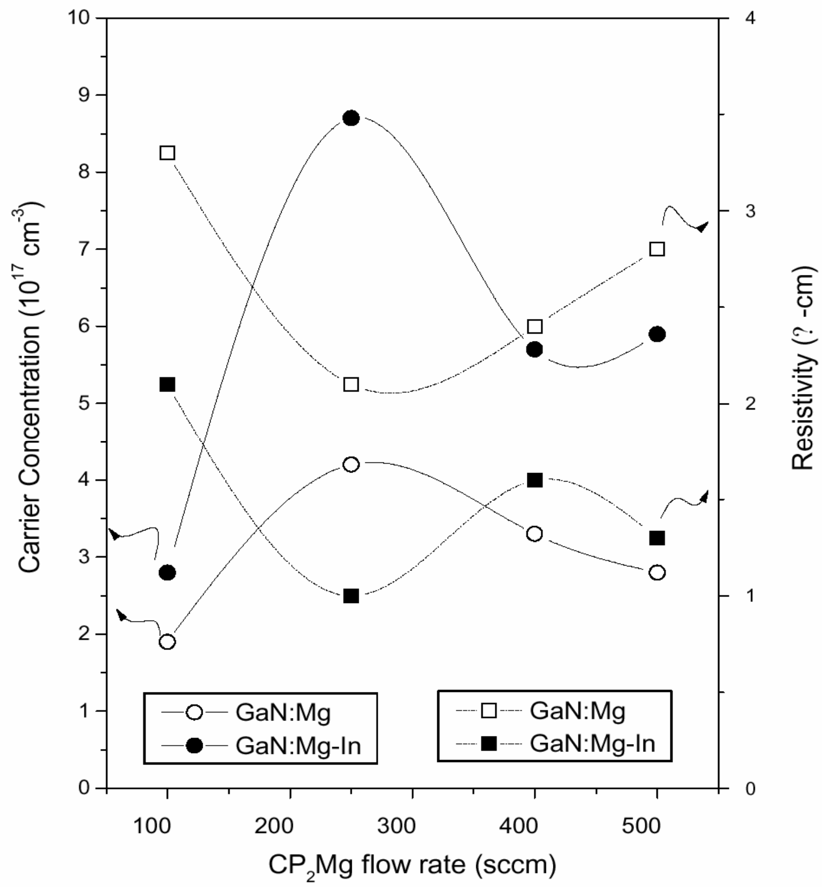

Fig 4.3. Hall properties of p-type GaN and In-Mg codoped GaN films as a function of Mg source flow rate.

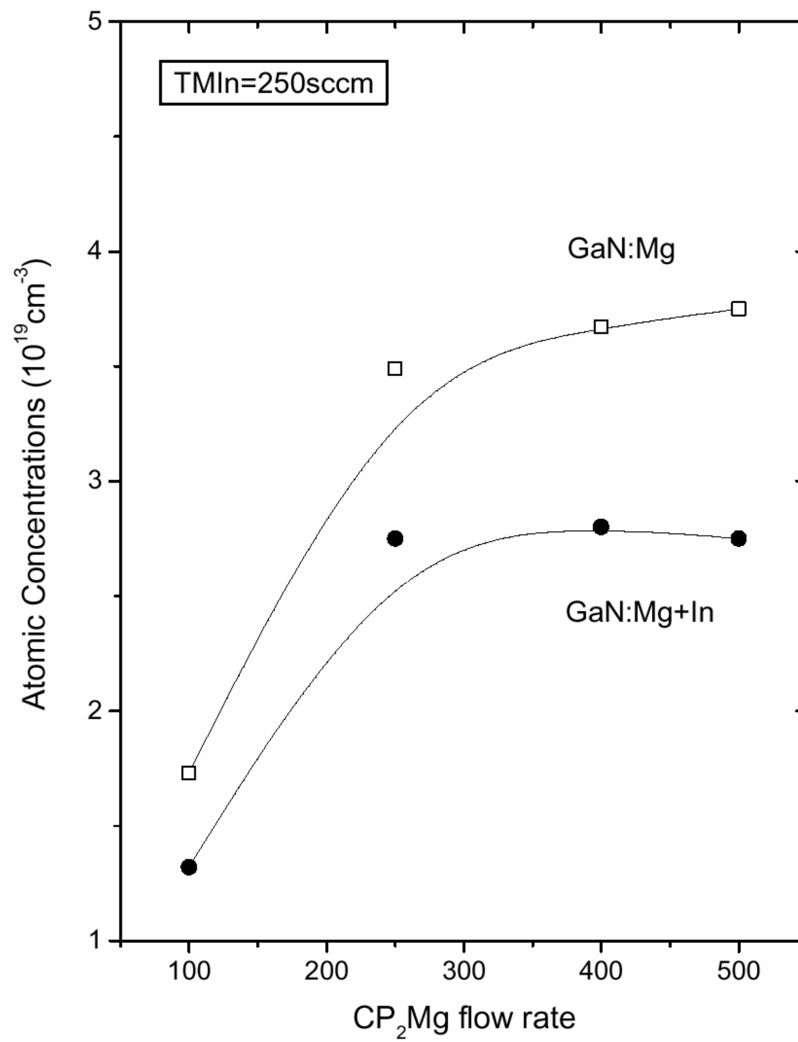

Fig. 4.4. Results of SIMS data for the solid Mg concentration for p-GaN and In-Mg codoped GaN films.

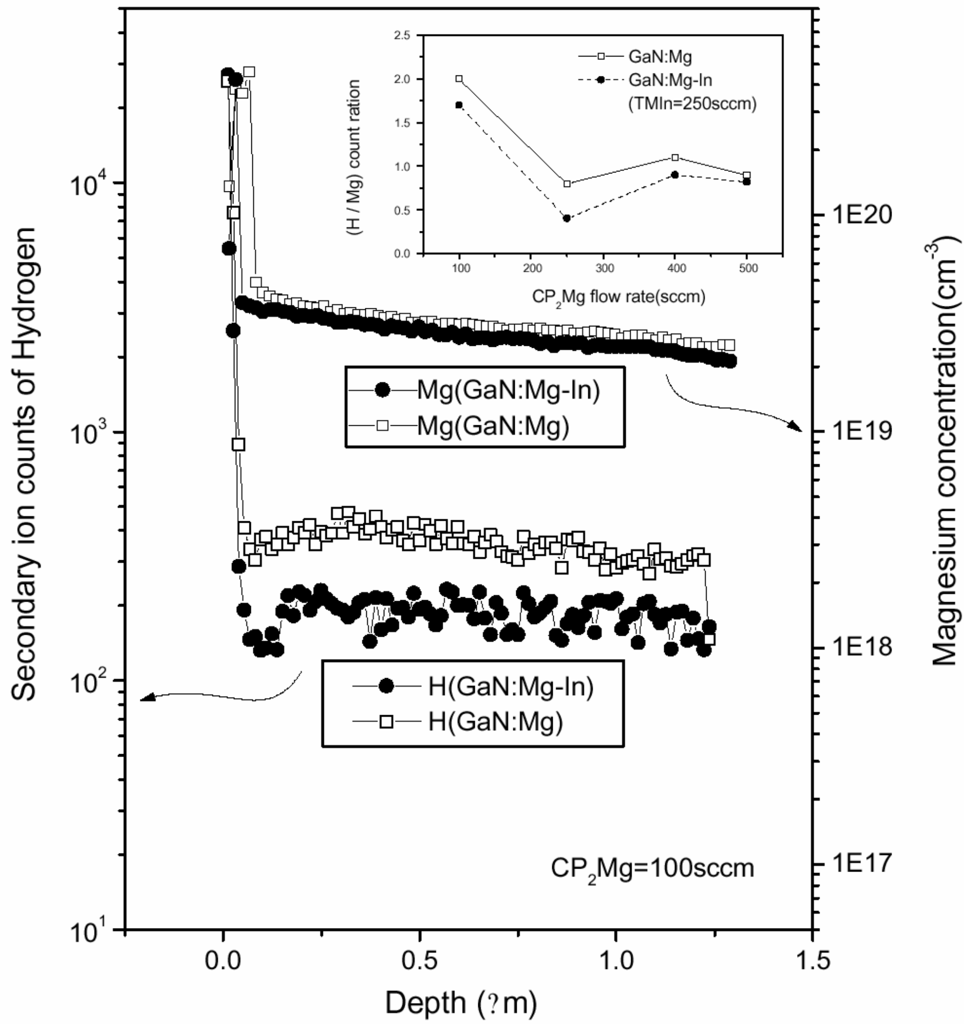

Fig 4.5. SIMS depth profile of Mg concentrations for both pure Mg-doped and In-Mg codoped GaN films.

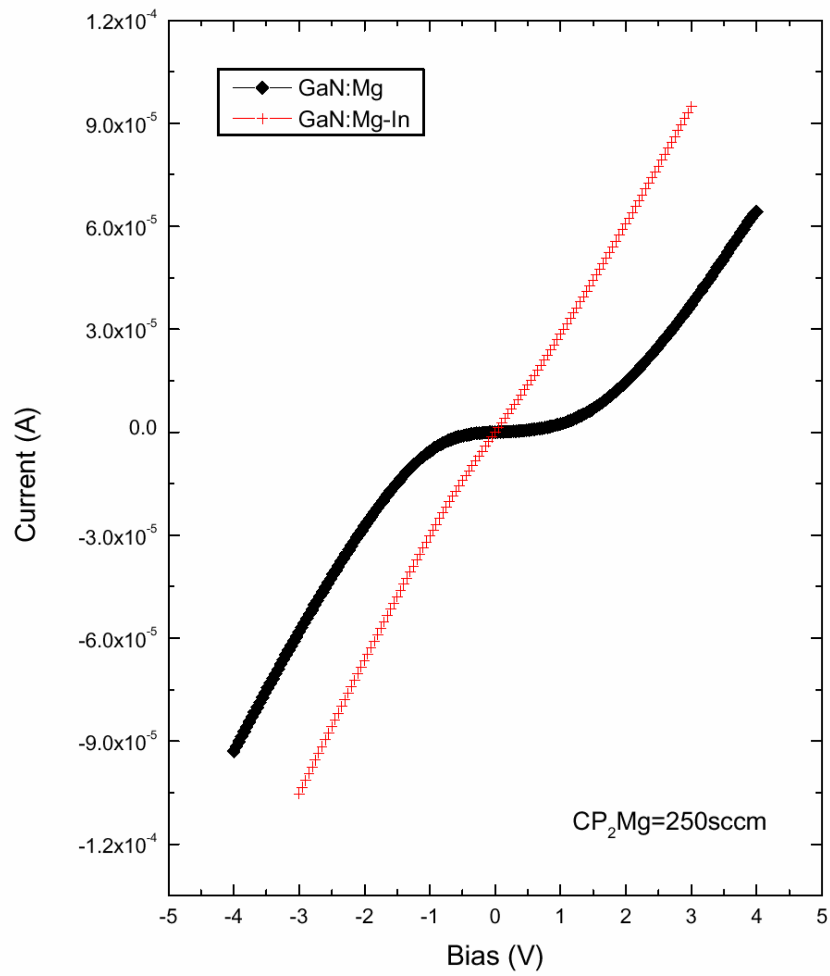

Fig. 4.6. I - V characteristics of as-deposited Mg-doped and In-Mg codoped GaN films without any dehydrogenation treatment.

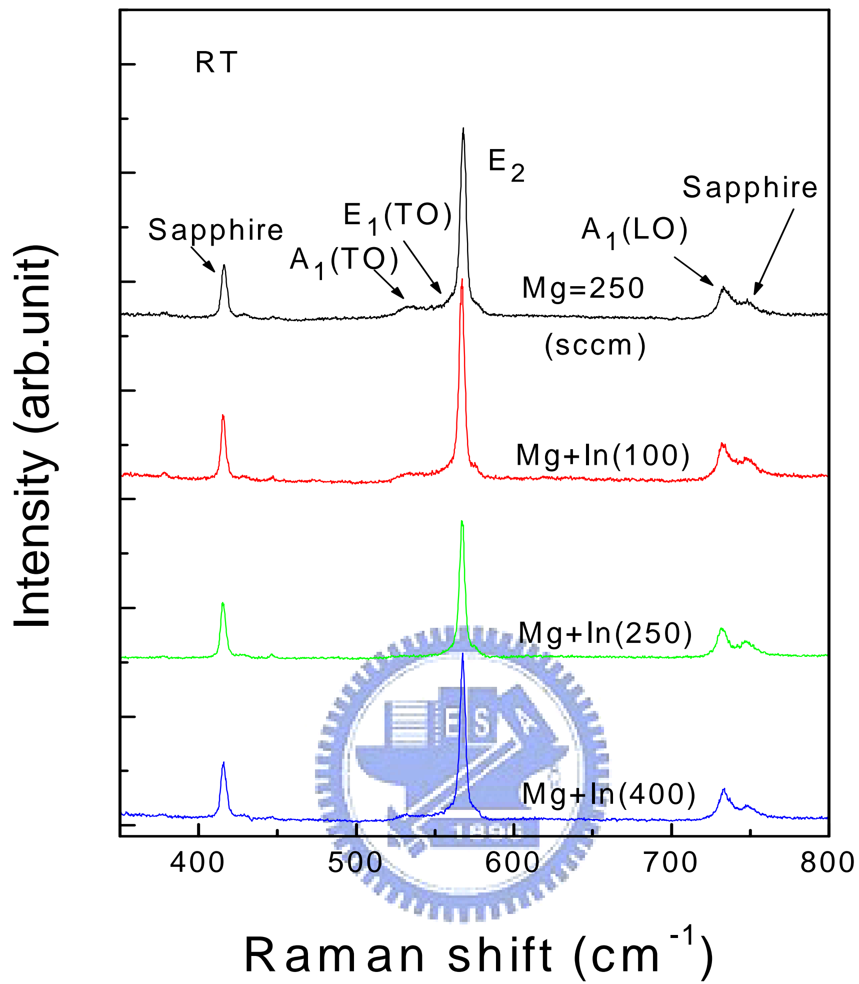

Fig . 4.7 Raman spectra of GaN:Mg and In-doped GaN:Mg films. Isoelectronic doping does not form alloy and clear carrier-induced plasmon since A_1(LO) persists.

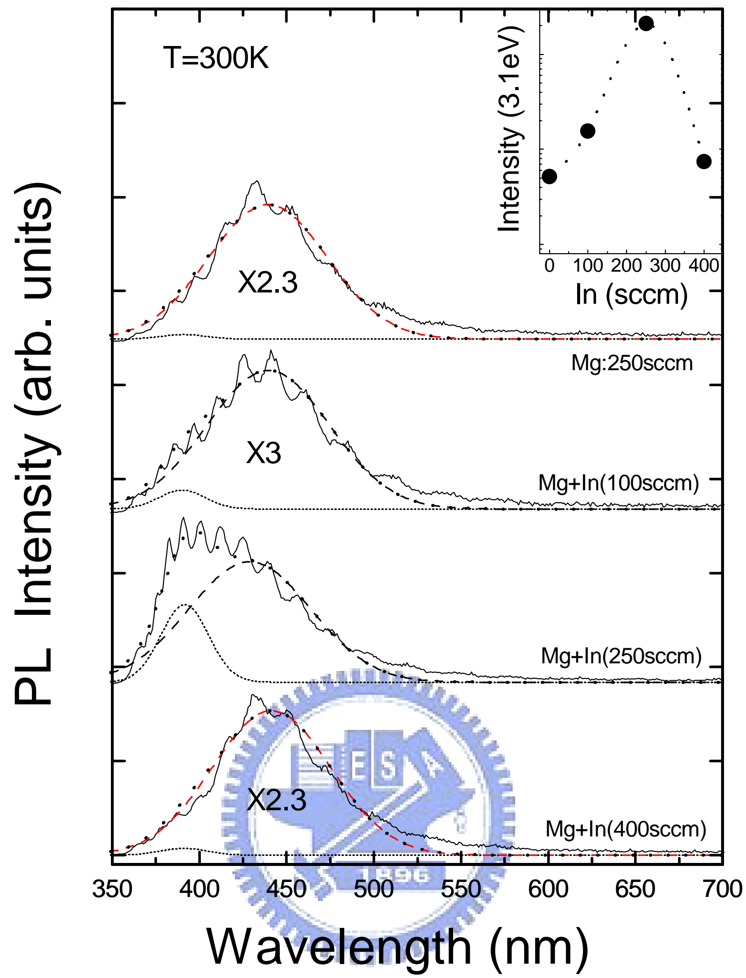

Fig. 4.8 The PL spectra of GaN:Mg and In-doped GaN:Mg films obtained at room temperature under different TMIn flow rates.

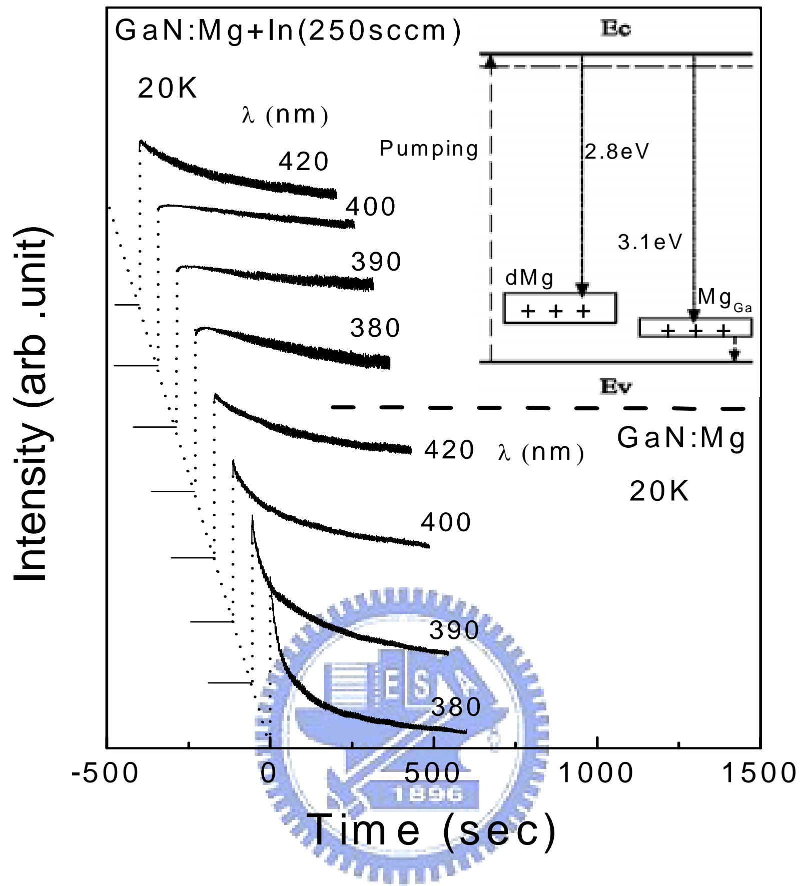

Fig. 4.9 PL intensity evolutions of GaN:Mg and In doped into GaN:Mg at different wavelengths.

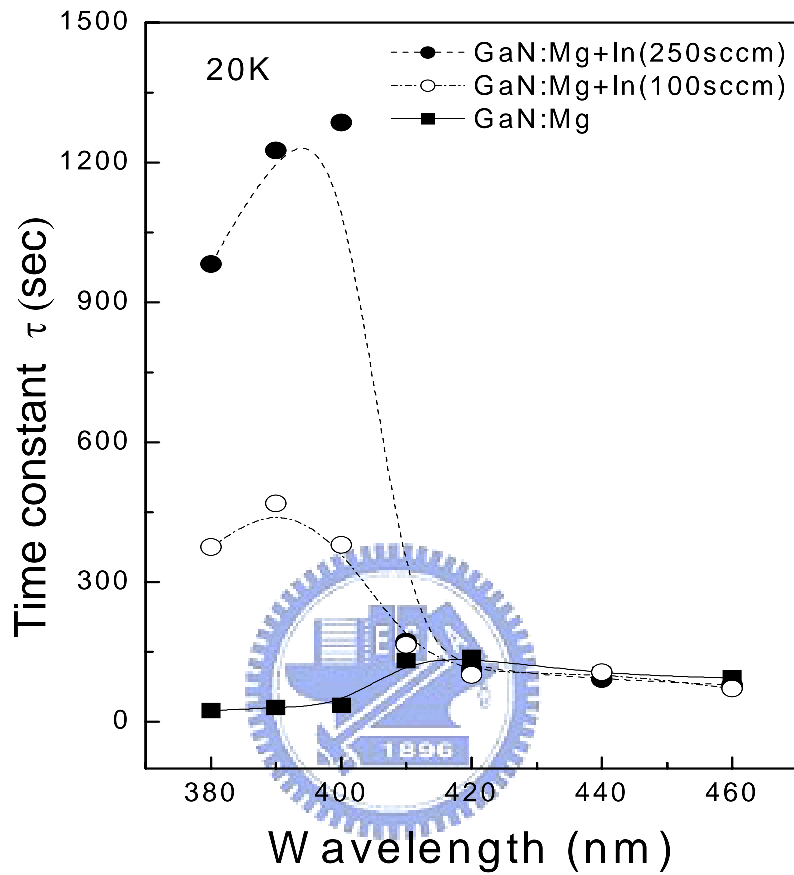

Fig. 4.10 The time constants of GaN:Mg and In-doped GaN:Mg films at various wavelengths for different TMIn flow rates.

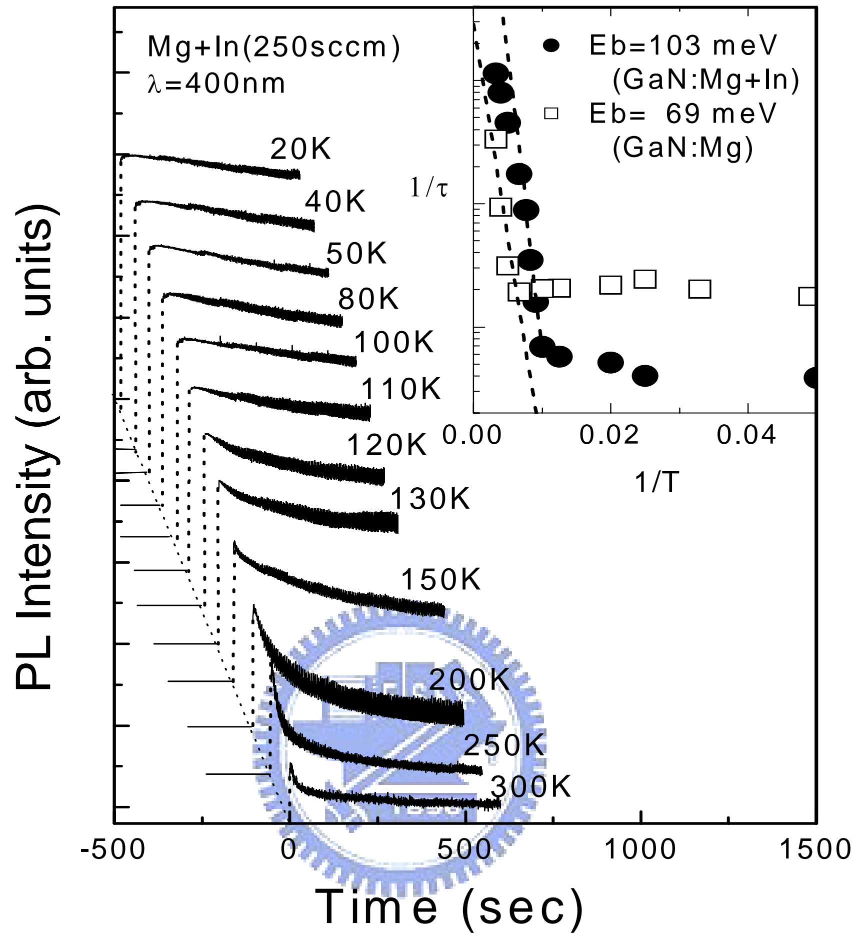

Fig. 4.11 PL intensity evolution at 400nm vs. temperature. The inset shows an Arrehenius plot that gives barrier energies of 69±8, 103±7 meV for GaN:Mg and In-doped GaN:Mg films, respectively.